The Influence of PbI₂ on Characteristic of Organic-Inorganic Hybrid Perovskite Thin Films

Yuze Peng, Yuxiang Wu, Linlin Tang, Juan Li, Jian Xu, Yangyang Du, Like Huang, Hongkun Cai, Jian Ni, Jianjun Zhang

Institute of Photo-Electronics, Nankai University, The Tianjin Key Laboratory for Optical-Electronic Thin Film Devices and Technology, Tianjin, China
Email: lj1018@nankai.edu.cn

Abstract

Organic-inorganic hybrid perovskite materials have attracted significant research efforts because of their outstanding properties. Meanwhile the crystallization of organic-inorganic hybrid perovskite materials can significantly influence the films quality. Here, we research the influence of the characteristics of PbI₂ thin film on final perovskite films and the mechanisms of film formation based on the two-step sequential deposition method. We found that the characteristics of PbI₂ thin film, such as the grain size, the grain shape, the surface roughness and the film densification, have significant effects on the final perovskite films due to different film crystallization process. According to the analysis on the characteristics of the perovskite films obtained from different PbI₂ precursor, we suggested that the formation of perovskite film begins from the PbI₂ crystals expanding when they are converted to MAPbI₃ perovskite by migration of MA+ cations from the grain boundaries.

Keywords

Perovskite, Film Formation, Grain Characteristics

1. Introduction

Organic-inorganic hybrid perovskite materials have attracted substantial attention because of their excellent physical properties [1] [2] [3] [4] [5], which enable them to be employed in solar cells and other application, such as LED. These materials show remarkable optical absorptions across a wide range of the solar spectrum, and a sharp optical band edge, which suggests low levels of disorder

[6] [7]. They also exhibit long charge-carrier diffusion lengths (>1 mm) relative to the absorption depth of incident light (~100 nm), [8] [9] meaning that almost all photoexcited species in the perovskite are able to reach the interfaces from where the charges are then transported through suitable hole- and electron-transporting layers to the electrodes. Based on these excellent properties, the power conversion efficiencies of organic-inorganic hybrid perovskite solar cells have increased from around 4% to a certified 22% in the last three years [1] [2] [3]. Now, most of the significant improvements in PCE have been a direct result of improvements in the formation of perovskite films, [10] [11] which led to a better film uniformity and crystalline quality, thus suggesting that the thin film features are of the upmost importance for achieving high performance.

As we know, organic-inorganic hybrid perovskites are a family of materials that share a crystal structure with calcium titanate, that is, ABX_3. These material are crystallized from organic halide and metal halide salts to form crystals in the ABX_3 structure, where A is the organic cation, such as methylammonium (MA = $CH_3NH_3^+$), B is the metal cation, such as lead (B = Pb^{2+}) and X is the halide anion (X = I, Br, Cl or mixtures). As for this, there is a general schematic diagram of perovskite synthesis (**Figure 1**). And a lot of processing techniques of perovskite layers have been reported to obtain high-quality perovskite films so far, such as one-/two-step solution process, vacuum deposition, and solvent vapor/additive assisted crystal growth [12]-[18]. Although these methods give some help to understand the growth mechanisms of perovskite films, however the growth mechanisms of perovskite films are not completely clear. The two-step sequential deposition method in all method for film formation is more helpful for studying the growth mechanisms of perovskite crystallites.

We have found that the characteristics of PbI_2 layer play a significant role in the final perovskite films formation. In this paper, we research the influence of PbI_2 film characteristics on the final perovskite films and its mechanisms based on the two-step sequential deposition method.

2. Experimental Section

Many methods to fabricate organic-inorganic perovskites have emerged, each resulting in varying degrees of surface coverage [19], and crystal and film quality [20]. Nevertheless, the two-step sequential deposition method can achieve
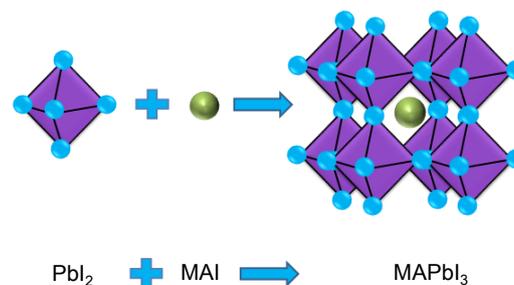

PbI_2 ➕ MAI ➡ $MAPbI_3$

Figure 1. Schematic illustration of synthesis of perovskite.

additional control over the morphology by sequentially depositing the two precursors relative to one-step deposition [21]. Meanwhile the two-step sequential deposition method is more flexible to design the procession of film formation. Here, organic-inorganic perovskite films were fabricated by two-step sequential deposition methods, which is helpful to investigate the effect of PbI_2 layer characteristics on the perovskite films formation.

2.1. Organic-Inorganic Perovskite Thin Films Deposition

2.1.1. PbI₂ Layer Fabricated by Spin Coatings

Here, the inorganic framework film was formed by depositing PbI_2 solution on the substrates. PbI_2 solution was prepared in DMF. The prepared PbI_2 solution was preheated at 110°C on a hot plate, followed by spin coating on the substrates at 4000 rpm for 40 s, then the PbI_2 film was put back on the hot plate for 15 min of drying. To obtain the perovskite thin film, substrates with PbI_2 film were then put into a vacuum coating machine, then MAI was deposited by thermal evaporation for 30 min (Figure 2). After cooling down to room temperature, these perovskite thin films were annealed for 18 min at 100°C. Then the films were rinsed with 2-propanol, and dried under a flow of clean air.

2.1.2. PbI₂ Layer Fabricated by Thermal Evaporation

This method to convert PbI_2 to a perovskite is aside from conversions in solution, where the substrate is exposed to the PbI_2 vapor. Then substrates with PbI_2 film were then put into a vacuum coating machine, then MAI was deposited by thermal evaporation for 30 min, sequentially (Figure 3). After cooling down to
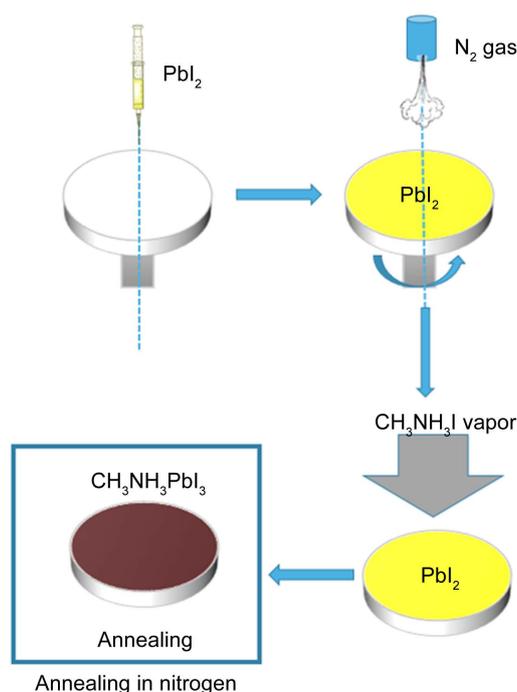

Figure 2. Schematic illustration of the procedure of perovskite thin film prepared via modified vapor-assisted solution process.
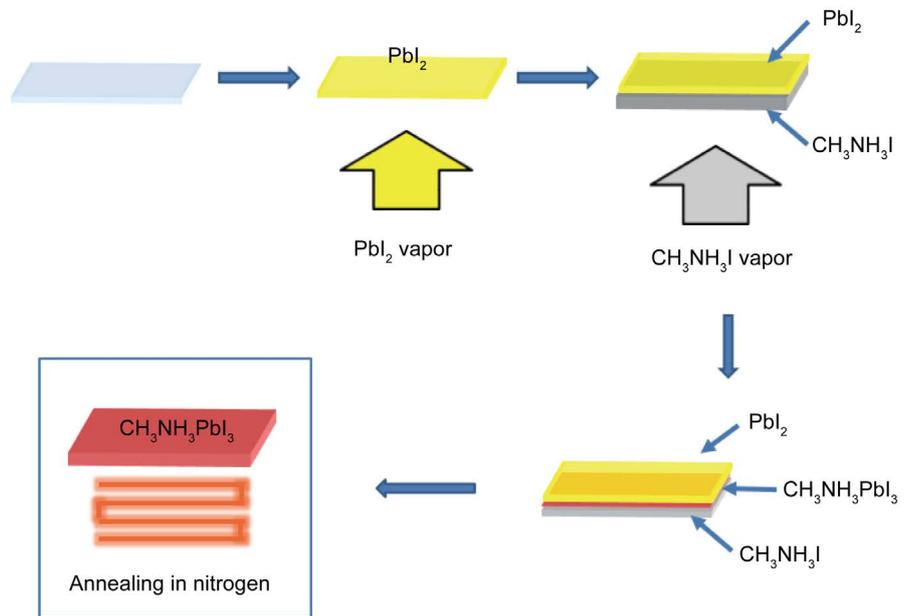
Figure 3. Schematic illustration of the procedure of perovskite thin film prepared via sequential thermal evaporation process.

room temperature, the perovskite films were annealed for 30 min at 100°C. Then the films are rinsed with 2-propanol, and dried under a flow of clean air.

2.2. Analysis of Characteristics of the Resulted Layers

The crystal structures of the $CH_3NH_3PbI_3$ films were characterized by X-ray diffraction (XRD, Philips PANalytical X'Pert Pro) with a copper X-ray source, and the surface morphologies were observed by scanning electron microscope (SEM, Hitachi SU8010) and atomic force microscopy (AFM) (Seiko SPA-400SPM UNIT). All samples were tested in air and at room temperature.

3. Results and Discussions

To investigated the characteristics of PbI_2 layer prepared by different processes. We prepared different PbI_2 layers by spin coating and thermal evaporation, respectively.

3.1. The Characteristics of PbI₂ Layer Prepared by Different Processes

As our previous work described [22], SEM and XRD measurements of PbI_2 layers fabricated by spin coating with different solution concentrations were taken. In **Figures 4(f)-(j)**, an obvious signature peak at 12.65° is observed in all PbI_2 layers, which indicate doubtless PbI_2 material. **Figures 4(a)-(e)** show the top-view SEM images of PbI_2 films with the different solution concentration. It is observed that the PbI_2 layer has no clear morphology and fuzzy domain boundaries with low PbI_2 solution concentration (**Figure 4(a)**). With the increase of PbI_2 solution concentration, the morphology of PbI_2 layer becomes
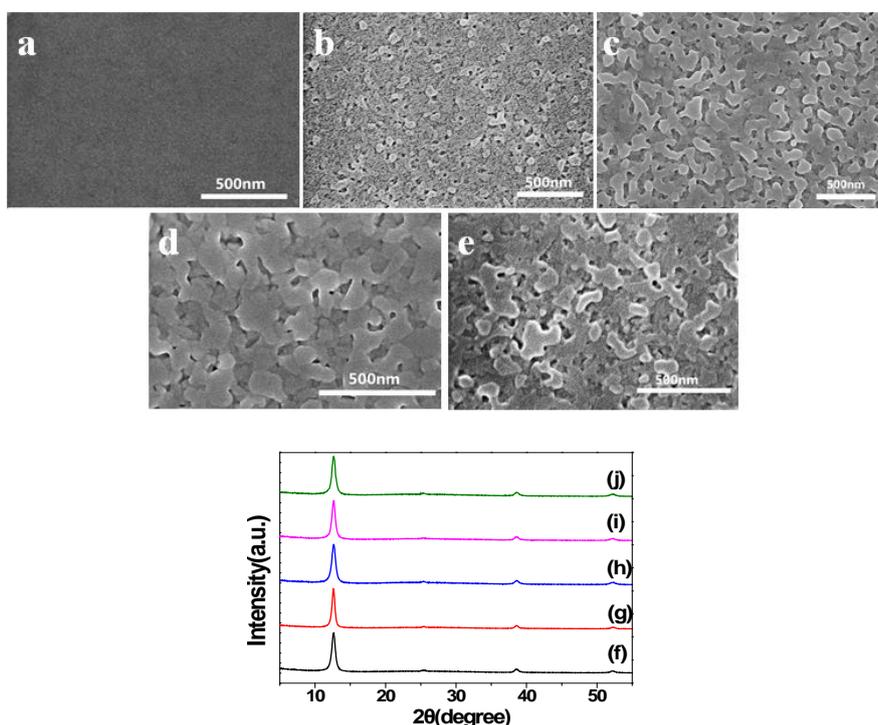
Figure 4. SEM top-view images and X-ray diffraction pattern of PbI$_2$ films: PbI$_2$ solution concentration varied from 100 (mg/mL) (a,f), 250 (mg/mL) (b,g), 285 (mg/mL) (c,h), 345 (mg/mL) (d,i), 500 (mg/mL) (e,j).

gradually clear (**Figures 4(a)-(e)**) with pancake-shape crystalline grain, the grain size gradually increases as shown in **Figures 4(a)-(e)**. Meanwhile, the surface roughness also gradually increases as extracted from its AFM measurements (see **Table 1**), which is consistent with SEM measurements (**Figures 4(f)-(j)**). We found the PbI$_2$ grains prepared by spin coating have fuzzy domain boundaries.

Then, the characteristics of PbI$_2$ layer fabricated by thermal evaporation with different amount of PbI$_2$ were researched via the SEM images and XRD measurements in **Figure 5**. However, we found the PbI$_2$ layers by thermal evaporation appeared a completely different morphology from that by spin coating. As shown in **Figure 5**, all the PbI$_2$ layers obtained by thermal evaporation have clear surface morphology and appear rice-shaped crystalline grain. With the increase of the amount of PbI$_2$, the surface roughness and the grain size of PbI$_2$ layers gradually increases. On the other hand, the sharp signature peak at 12.65° in the XRD measurements implies well crystalline degree of all PbI$_2$ layers obtained via thermal evaporation (**Table 2**).
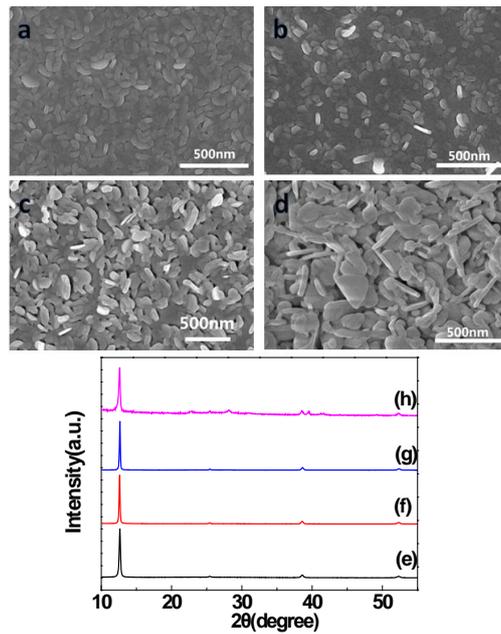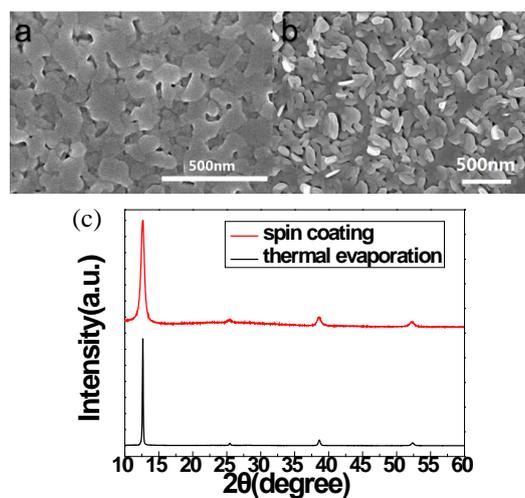
The SEM images and XRD measurements of twos representative PbI$_2$ layers prepared by spin coating and thermal evaporation are compared as shown in **Figure 6**. As can be seen, there has an obvious difference between the morphology of the two types of PbI$_2$ layers. The later has a clear crystal shape and a loose structure comparing with that of the former. However the former have fuzzy domain boundaries and fewer grain boundaries than the later. From the XRD measurements in **Figure 6(c)**, the sharpness of XRD peak of the PbI$_2$ layers

Table 1. Parameters derived from AFM measurements corresponding to Figures 4(a)-(e).

Roughness surface RMS (nm)	100 mg/mL	250 mg/mL	285 mg/mL	345 mg/mL	500 mg/mL
PbI_2 films	7.184E−01	2.029E+00	1.255E+00	1.852E+00	6.035E+00

Table 2. Parameters derived from AFM measurements corresponding to Figures 5(a)-(d).

Roughness surface RMS (nm)	30 mg	60 mg	90 mg	120 mg
PbI_2 films	5.998	1.367E+01	2.543E+01	3.745E+01

Figure 5. SEM top-view images and X-ray diffraction pattern of PbI_2 films: the amount of PbI_2 varied from 30 (mg) (a,e), 60 (mg) (b,f), 90 (mg) (c,g), 150 (mg) (d,h).

Figure 6. Scanning electron microscope (SEM) images and (a) by spin coating with 345 (mg/mL) PbI_2 solution, and prepared (b) by thermal evaporation with 90 (mg) PbI_2 power, respectively. (c) X-ray diffraction pattern of representative PbI_2 layer prepared.

fabricated by two methods has a significant difference, where the peaks corresponding to PbI_2 obtained by thermal evaporation process is very sharp than that by spin-coating process, illustrating the higher crystalline degree of the PbI_2 obtained by thermal evaporation process.

3.2. The Influence of PbI_2 Characteristics on Final Organic-Inorganic Hybrid Perovskite Films

To investigate the influence of characteristics of PbI_2 film on final perovskite films, we fabricated perovskite films with different PbI_2 precursor. **Figure 7** shows the SEM images of perovskite films made from the PbI_2 precursor fabricated by spin coating with different solution concentrations above discussion, with the increase of PbI_2 solution concentration, the film surface roughness gradually increases, which benefit PbI_2 to contact MAI and convert completely to perovskite. Then the final perovskite films were obtained without PbI_2 residue, as illustrated in **Figure 7(i)**, **Figure 7(j)**, where the PbI_2 solution concentration is higher than 345 mg/ml. As to the PbI_2 solution concentration below 250 mg/ml, the perovskite films did not have PbI_2 residue, which were mainly due to lower PbI_2 solution concentration (see **Figure 7(f)**, **Figure 7(g)**). Nevertheless, the grain sizes of perovskite films obtained with different PbI_2 solution concentration are almost same (**Figures 7(a)-(e)**). Additionally, the surface of PbI_2 layer would become rough (see **Figure 4(e)** and **Table 1**) when the PbI_2 solution
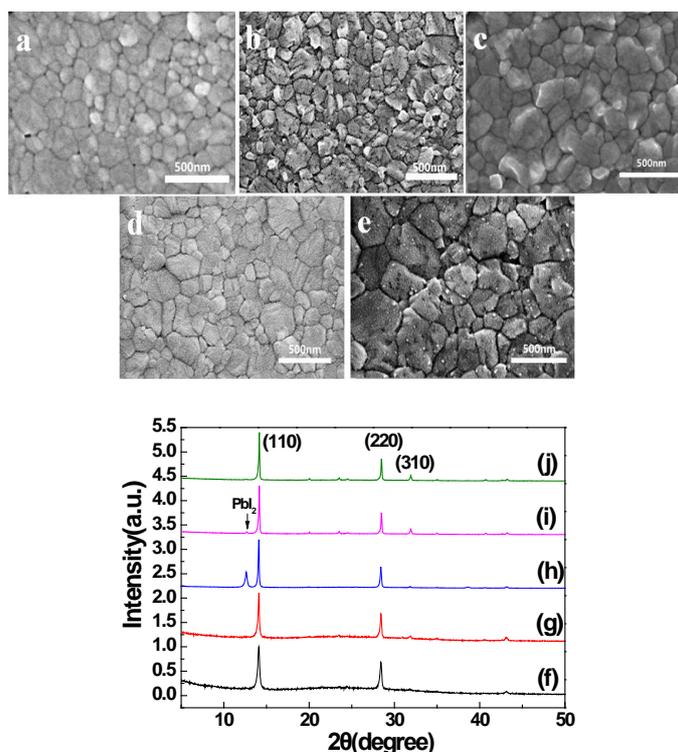

Figure 7. SEM top-view images and X-ray diffraction pattern of MAPbI$_3$ films: PbI$_2$ solution concentration varied from (100 mg/mL) (a,f), 250 (mg/mL) (b,g), 285 (mg/mL) (c,h), 345 (mg/mL) (d,i), 500 (mg/mL) (e,j).

concentration is too high, finally leading to a rough and irregular surface of perovskite film when PbI_2 layer converts to perovskite films (see **Figure 7(e)**). Therefore, we suggest that the characteristics of PbI_2 layers fabricated by spin coating have a main influence on the roughness of perovskite film rather than the grain size.

Figure 8 shows the scanning electron microscope (SEM) images of perovskite films made from the PbI_2 precursor by thermal evaporation with different amount of PbI_2. Comparing with the PbI_2 film fabricated by spin coating, the PbI_2 films fabricated by thermal evaporation have loose morphologies as shown above, which make it easier for the MAI to diffuse into PbI_2 films and makes complete reaction between the MAI and PbI_2. Therefore, PbI_2 residue in the final films is fewer than that made from the spin coating PbI_2 precursor as shown in **Figure 8(e)**. However when the amount of PbI_2 reaches to 150 mg, an obvious signature peak at 12.65° appears, which suggests that the amount of PbI_2 was too much to react completely and there is some PbI_2 residue in the final perovskite films. Different with the case of spin coating PbI_2 precursor, the characteristics of PbI_2 film have an effect on both the grain size and the film surface roughness final perovskite films.

Base on the above analysis, we found the final perovskite films are very dependent on the characteristics of PbI_2 precursor with respect to the morphology, the grain size and crystalline degree. Because the PbI_2 prepared by spin coating
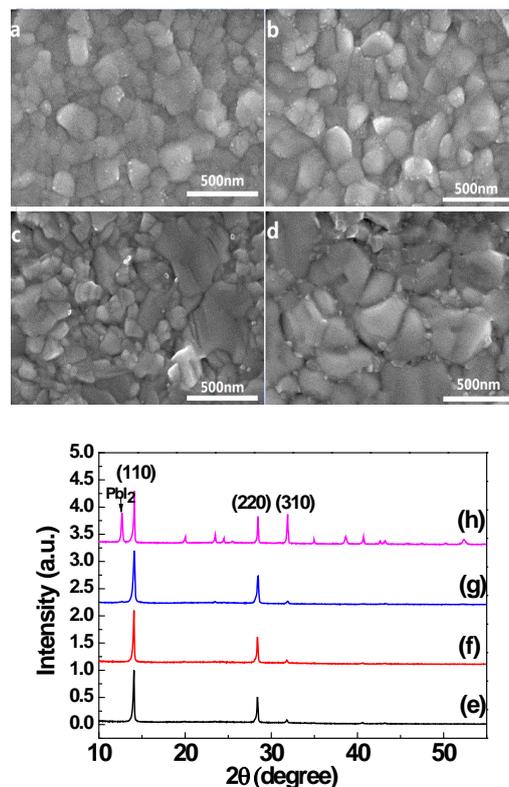

Figure 8. SEM top-view images and X-ray diffraction pattern of $MAPbI_3$ films: the amount of PbI_2 varied from 30 (mg) (a,e), 60 (mg) (b,f), 90 (mg) (c,g), 150 (mg) (d,h).

has less grain boundary than that prepared by thermal evaporation, the final perovskite films obtained by thermal evaporation (Figure 8) have smaller grain size than that obtained by spin coating (Figure 7). As we know, the perovskite formation process is the combination of an organic component, such as methylammonium iodide (MAI), with an inorganic component, such as PbI_2 or $PbCl_2$, to form the perovskite ($MAPbI_3$ or $MAPbI_{3-x}Cl_x$, respectively). We suggested that the formation of perovskite in two-step method is the PbI_2 as nucleus reacts with MAI, in the meantime, the PbI_2 crystals start to expand to convert to $MAPbI_3$ crystals by migration of MA+ cations from the grain boundaries. Then the PbI_2 deposited via thermal evaporation has high grain density as the nucleus which grows into perovskite grains, resulting in high perovskite grain density and smaller grain size. As to the PbI_2 deposited via spin coating, grains have fuzzy domain boundaries and fewer grain boundaries, therefore, the final perovskite film has lower grain density and larger grain size when PbI_2 crystals are converted to $MAPbI_3$ perovskite by migration of MA+ cations from the grain boundaries. The cross-sectional SEM images of $MAPbI_3$ perovskite made from different PbI_2 precursor are shown in Figure 9: It can be observed that the crystalline structure of $MAPbI_3$ perovskite thin film prepared by spin coating fused together (Figure 9(a)), nevertheless, that by thermal evaporation has clear grain boundaries and crystal piled up together (Figure 9(b)), which is consistent with the above results and analysis.

4. Conclusions

In summary, we have found that the PbI_2 thin film has different characteristics fabricated by different process based on the two-step sequential deposition method. The PbI_2 thin film fabricated by thermal evaporation usually has a clear crystal shape and a loose structure comparing with that by spin coating. However, the latter has fuzzy domain boundaries and fewer grain boundaries than the former. The final perovskite films are very dependent on the characteristics of PbI_2 precursor. We suggest that the characteristics of PbI_2 layers fabricated by spin coating mainly influence on the roughness of perovskite film rather than the grain size, while, the characteristics of PbI_2 film have an effect on both the grain size and the film surface roughness of the final perovskite films. So, when perovskite applied to TFTs as active layer, in order to make carrier mobility maximized, we need a bigger grain size and higher coverage. Thus, the research
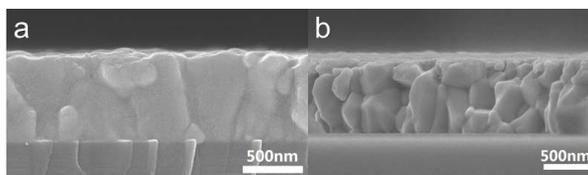

Figure 9. Cross-sectional view SEM images of $MAPbI_3$ perovskite prepared (a) by spin coating with 345 (mg/mL) PbI_2 solution, and (b) by thermal evaporation with 90 mg PbI_2 power, respectively.

of influence of PbI$_2$ on characteristic of perovskite thin films is important and meaningful.

We suggested the formation of perovskite is that the PbI$_2$ crystals as the nucleus start to grow into perovskite grains, where they reacted with MAI to convert to MAPbI$_3$ by migration of MA+ cations from the grain boundaries. The high-quality perovskite films can be achieved by adjusting the PbI$_2$ crystallization.

Acknowledgements

References

[1] Noh, J.H., Yang, W.S., Kim, Y.C., Ryu, S., Seo, J. and Seok, S.I. (2015) Compositional Engineering of Perovskite Materials for High Performance Solar Cells. *Nature*, **517**, 476-480. https://doi.org/10.1038/nature14133

[2] Huang, F.Z., Dkhissi, Y., Huang, W.C., Xiao, M.D., Benesperi, I., Rubanov, S., Zhu, Y., Lin, X.F., Jiang, L.C., Zhou, Y.C., Gray-Weale, A., Etheridge, J., McNeill, C.R., Caruso, R.A., Bach, U., Spiccia, L. and Cheng, Y.-B. (2014) Gas-Assisted Preparation of Lead Iodide Perovskite Films Consisting of a Monolayer of Single Crystalline Grains for High Efficiency Planar Solar Cells. *Nano Energy*, **10**, 10-18. https://doi.org/10.1016/j.nanoen.2014.08.015

[3] Goetzberger, A. and Hebling, C. (2000) Photovoltaic Materials, Past, Present, Future. *Solar Energy Materials and Solar Cells*, **62**, 1-19. https://doi.org/10.1016/S0927-0248(99)00131-2

[4] Green, M.A., Emery, K., Hishikawa, Y., Warta, W. and Dunlop, E.D. (2015) Solar Cell Efficiency Tables. *Progress in Photovoltaics: Research and Applications*, **23**, 1-9. https://doi.org/10.1002/pip.2573

[5] Kojima, A., Teshima, K., Shirai, Y. and Miyasaka, T. (2009) Organometal Halide Perovskites as Visible-Light Sensitizers for Photovoltaic Cells. *Journal of the American Chemical Society*, **131**, 6050-6051. https://doi.org/10.1021/ja809598r

[6] De Wolf, S., Holovsky, J., Moon, S.-J., Löper, P., Niesen, B., Ledinsky, M., Haug, F.-J., Yum, J.-H. and Ballif, C. (2014) Organometallic Halide Perovskites: Sharp Optical Absorption Edge and Its Relation to Photovoltaic Performance. *The Journal of Physical Chemistry Letters*, **5**, 1035-1039. https://doi.org/10.1021/jz500279b

[7] De Wolf, S., Holovsky, J., Moon, S.-J., Löper, P., Niesen, B., Ledinsky, M., Haug, F.-J., Yum, J.-H. and Ballif, C. (2014) Preparation of Single-Phase Films of CH$_3$NH$_3$Pb(I$_{1-x}$Br$_x$)$_3$ with Sharp Optical Band Edges. *The Journal of Physical Chemistry Letters*, **5**, 2501-2505. https://doi.org/10.1021/jz501332v

[8] Stranks, S.D., Eperon, G.E., Grancini, G., Menelaou, C., Alcocer, M.J.P., Leijtens, T., Herz, L.M., Petrozza, A. and Snaith, H.J. (2013) Electron-Hole Diffusion Lengths Exceeding 1 Micrometer in an Organometal Trihalide Perovskite Absorber. *Science*, **342**, 341-344. https://doi.org/10.1126/science.1243982

[9] Xing, G.C., Mathews, N., Sun, S.Y., Lim, S.S., Lam, Y.M., Grätzel, M., Mhaisalkar, S. and Sum, T.C. (2013) Long-Range Balanced Electron- and Hole-Transport Lengths

in Organic-Inorganic CH₃NH₃PbI₃. *Science*, **342**, 344-347.
https://doi.org/10.1126/science.1243167

[10] Jeon, N.J., Noh, J.H., Kim, Y.C., Yang, W.S., Ryu, S. and Seok, S.I. (2014) Solvent Engineering for High-Performance Inorganic-Organic Hybrid Perovskite Solar Cells. *Nature Materials*, **13**, 897-903. https://doi.org/10.1038/nmat4014

[11] Zhou, H.P., Chen, Q., Li, G., Luo, S., Song, T.-B., Duan, H.-S., Hong, Z.R., You, J.B., Liu, Y.S. and Yang, Y. (2014) Interface Engineering of Highly Efficient Perovskite Solar Cells. *Science*, **345**, 542-546. https://doi.org/10.1126/science.1254050

[12] Liu, M.Z., Johnston, M.B. and Snaith, H.J. (2013) Efficient Planar Heterojunction Perovskite Solar Cells by Vapour Deposition. *Nature*, **501**, 395-398. https://doi.org/10.1038/nature12509

[13] Chen, Q., Zhou, H., Hong, Z., Luo, S., Duan, H.S., Wang, H.H., Liu, Y., Li, G. and Yang, Y. (2014) Planar Heterojunction Perovskite Solar Cells via Vapor-Assisted Solution Process. *Journal of the American Chemical Society*, **136**, 622-625. https://doi.org/10.1021/ja411509g

[14] Gao, C., Liu, J., Liao, C., Ye, Q., Zhang, Y., He, X., Guo, X., Mei, J. and Lau, W. (2015) Formation of Organic-Inorganic Mixed Halide Perovskite Films by Thermal Evaporation of PbCl₂ and CH₃NH₃I Compounds. *RSC Advances*, **5**, 26175-26180. https://doi.org/10.1039/C4RA17316C

[15] Xiao, Z., Dong, Q., Bi, C., Shao, Y., Yuan, Y. and Huang, J. (2014) Solvent Annealing of Perovskite-Induced Crystal Growth for Photovoltaic Device Efficiency Enhancement. *Advanced Materials*, **26**, 6503-6509. https://doi.org/10.1002/adma.201401685

[16] Liang, P.W., Liao, C.Y., Chueh, C.C., Zuo, F., Williams, S.T., Xin, X.K., Lin, J. and Jen, A.K. (2014) Additive Enhanced Crystallization of Solution-Processed Perovskite for Highly Efficient Planar-Heterojunction Solar Cells. *Advanced Materials*, **26**, 3748-3754. https://doi.org/10.1002/adma.201400231

[17] Xie, F.X., Zhang, D., Su, H., Ren, X., Wong, K.S., Gratzel, M., and Choy, W.C. (2015) Vacuum-Assisted Thermal Annealing of CH₃NH₃PbI₃ for Highly Stable and Efficient Perovskite Solar Cells. *ACS Nano*, **9**, 639-646. https://doi.org/10.1021/nn505978r

[18] Dualeh, A., Tetreault, N., Moehl, T., Gao, P., Nazeeruddin, M.K., Gratzel, M. (2014) Effect of Annealing Temperature on Film Morphology of Organic-Inorganic Hybrid Perovskite Solid-State Solar Cell. *Advanced Functional Materials*, **24**, 3250-3258. https://doi.org/10.1002/adfm.201304022

[19] Ball, J.M., Lee, M.M., Hey, A., Snaith, H.J. (2013) Low-Temperature Processed Meso-Superstructured to Thin-Film Perovskite Solar Cells. *Energy & Environmental Science*, **6**, 1739-1743. https://doi.org/10.1039/c3ee40810h

[20] Liu, D., Gangishetty, M.K. and Kelly, T.L. (2014) Effect of CH₃NH₃PbI₃ Thickness on Device Efficiency in Planar Heterojunction Perovskite Solar Cells. *Journal of Materials Chemistry A*, 19873-19881. https://doi.org/10.1039/C4TA02637C

[21] Schlipf, J., Docampo, P., Schaffer, C.J., Körstgens, V., Bießmann, L., Hanusch, F., Giesbrecht, N., Bernstorff, S., Bein, T. and Müller-Buschbaum, P. (2015) A Closer Look into Two-Step Perovskite Conversion with X-Ray Scattering. *The Journal of Physical Chemistry Letters*, **6**, 1265-1269. https://doi.org/10.1021/acs.jpclett.5b00329

[22] Wu, Y.X., Li, J., Xu, J., Du, Y.Y., Huang, L.K., Ni, J., Cai, H.K. and Zhang, J.J. (2016) Organic-Inorganic Hybrid CH₃NH₃PbI₃ Perovskite Materials as Channels in Thin-Film Field-Effect Transistors. *RSC Advances*, **6**, 16243-16249. https://doi.org/10.1039/C5RA24154E